



Insight into the scavenger effect of LiF on extinction of a carboxylate group for mid-infrared transparent Y_2O_3 –MgO nanocomposite

Ho Jin Ma, Jung Hoon Kong, Do Kyung Kim*

Department of Materials Science and Engineering, Korea Advanced Institute of Science and Technology (KAIST), 291 Daehak-ro, Yuseong-gu, Daejeon 34141, Republic of Korea

ARTICLE INFO

Article history:
Received 4 April 2020
Accepted 3 May 2020

Keywords:
Transparent ceramics
 Y_2O_3 –MgO nanocomposite
Sintering additive
Spectroscopic analysis
Hot-press

ABSTRACT

Y_2O_3 –MgO nanocomposite is introduced for infrared transparent ceramics due to its superior optical and mechanical characteristics. However, severe optical scattering and unnecessary absorption in the near- and mid-infrared regions restrict the applications of this material. Here, a broad mid-infrared transparent Y_2O_3 –MgO nanocomposite is achieved for the first time through low temperature sintering using an LiF additive. The influence of LiF is successfully demonstrated on the mid-infrared transparency of the as-sintered and post-annealed nanocomposites. Spectroscopic analysis are also performed, and primary absorption factors of the Y_2O_3 –MgO transparent ceramics are revealed. This study is a step toward designing widely utilized transparent ceramics.

© 2020 Acta Materialia Inc. Published by Elsevier Ltd. All rights reserved.

The Y_2O_3 –MgO nanocomposite is a representative infrared transparent ceramic for infrared domes and windows in extremely harsh environment [1–3]. Since the Y_2O_3 –MgO nanocomposite has outstanding thermal and mechanical properties superior to mono-phase polycrystalline transparent ceramics, including Y_2O_3 , $MgAl_2O_4$ and AlON, it has been proposed as a candidate for suitable military applications [4]. However, severe grain boundary scattering induced by a large difference in the refractive index between two phases in the microstructure significantly deteriorates the transmittance in the short-wavelength region (UV, visible and near-infrared). Moreover, the Y_2O_3 –MgO nanocomposite shows an unavoidable intense absorption at $7\ \mu\text{m}$ that is due to residual carbon components or CO_2 generated during the sintering and post-annealing process. Various absorption peaks around $4.5\ \mu\text{m}$ create many problems when the nanocomposite is actually applied [5–7]. Because of a virtually restricted transparent wavelength region, the nanocomposite has been developed over a decade concentrating only on the improvement of transmittance at the near-infrared wavelength by minimizing the grain size [8], or at the significantly narrow mid-infrared region (3 – $5\ \mu\text{m}$) [9–12]. Furthermore, to date investigations into alleviating absorption by external and internal factors in the mid-infrared region are still barely under way.

LiF, as a sintering additive, is extensively used to improve the sinterability of a variety of transparent ceramics [13–15]. When LiF acts as a low-temperature sintering aid, it becomes a liquid phase and increases the mass transfer and grain boundary mobility during the sintering, so the domain size grows considerably [16]. In the case of the Y_2O_3 –MgO nanocomposite, unnecessary grain growth leads degradation of the short-wavelength transmittance, so LiF is not utilized at all. Furthermore, in the early literature, it was also not exactly known how LiF affects the mid-infrared transparency.

To our knowledge for the first time, a broad mid-infrared transparent Y_2O_3 –MgO nanocomposite has been developed through low temperature consolidation exploiting LiF as a sintering aid. We explored the influence of LiF on the mid-infrared transparency, especially absorption at $7\ \mu\text{m}$, of the as-sintered and post-annealed Y_2O_3 –MgO nanocomposite. We performed spectroscopic analyses and defined the absorption factors of the Y_2O_3 –MgO transparent ceramics.

The auto-ignition combustion method is well-known as an excellent strategy for synthesizing fine, homogeneous and high-purity nanoparticles (see supplementary information for detailed experimental methods) [17]. Fig. S1 shows the crystal structure and crystallinity of the synthesized Y_2O_3 –MgO nanoparticles and sintered bulk ceramics. The observed X-ray diffraction peaks obviously correspond to Y_2O_3 and MgO cubic phases. No impurities were detected when the sintering procedure was carried out. The crystallite size of the calcined particles was fine at about 16 nm calculated by Scherrer equation. No residual LiF or second phases were generated through collateral reaction with the nanocompos-

* Corresponding author at: Department of Materials Science and Engineering, Korea Advanced Institute of Science and Technology (KAIST), 291 Daehak-ro, Yuseong-gu, Daejeon 34141, Republic of Korea.
E-mail address: dkkim@kaist.ac.kr (D.K. Kim).

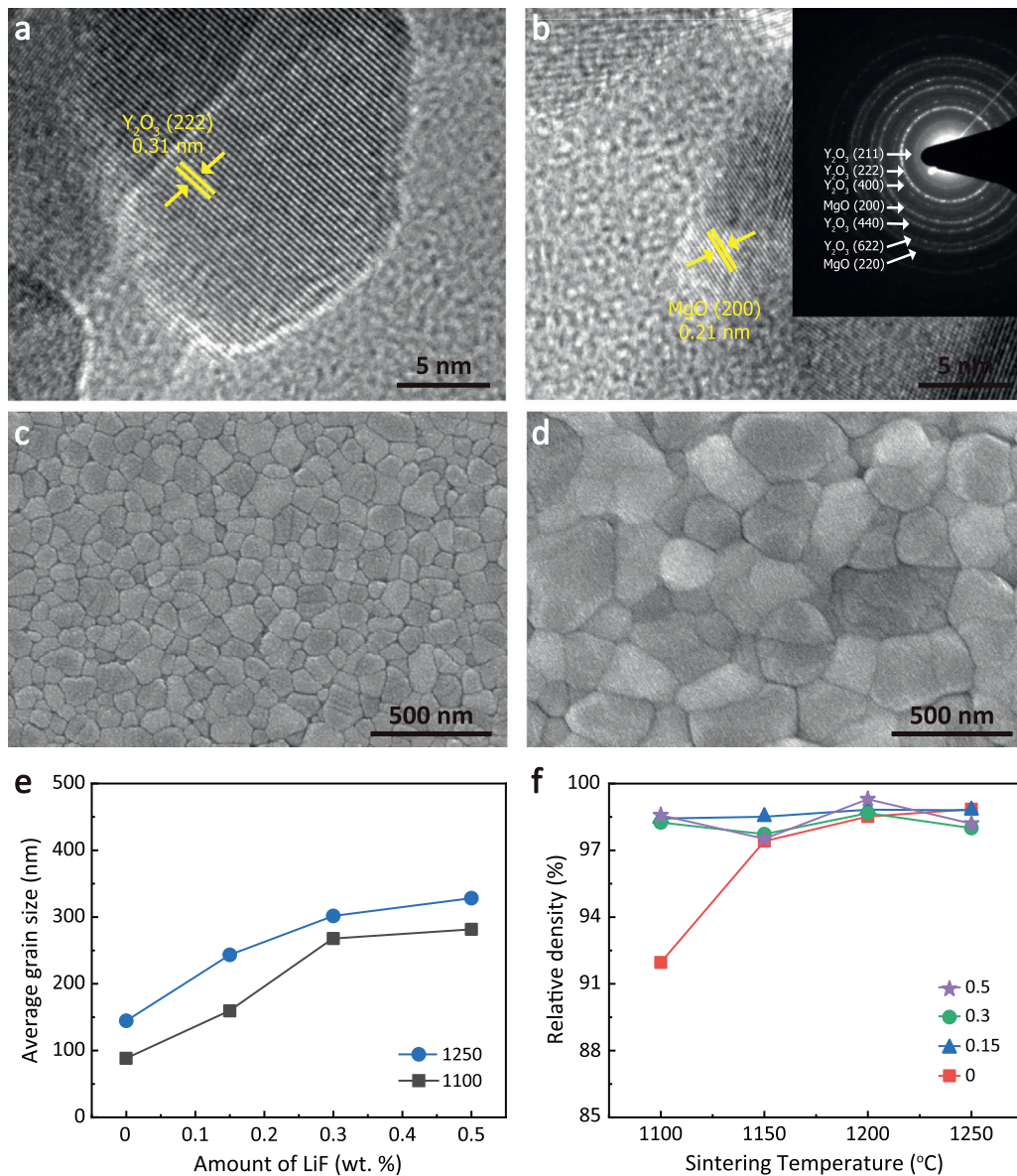


Fig. 1. (a, b) TEM images of the synthesized Y_2O_3 -MgO nanoparticles. The inset is the SAED pattern of the Y_2O_3 -MgO nanoparticles. SEM microstructure images of Y_2O_3 -MgO nanocomposite with different amounts of LiF sintering aid; (c) 0 and (d) 0.5 wt%. The samples were sintered at 1250 °C for 2 h. (e) The relative density and average grain size of sintered samples at 1100 and 1250 °C with different LiF concentrations. (f) The relative density of sintered samples with different concentrations and sintering temperatures.

ite. The morphology and crystallinity of the synthesized nanoparticles were observed from the TEM images, as can be seen in Fig. 1(a) and (b). The average particle size after calcination was less than 20 nm, which corresponded to the value from Scherrer equation. Lattice fringes were in agreement with the (222) plane of Y_2O_3 and the (200) plane of MgO phases, respectively. The results of TEM and SAED analysis of the nanoparticles involving 0.5 wt% LiF are shown in Fig. S2 in which it is difficult to distinguish the additive from the bare nanocomposite particles.

SEM microstructural images of nanocomposites with various amounts of LiF are represented in Fig. 1(c) and (d). The data represent discernible differences in the grain size of the sintered body according to the amount of LiF at the same consolidation conditions. As shown in Fig. 1(c), when the nanocomposite was sintered at 1250 °C, fine grains with a size of 144 nm can be achieved. With an increasing amount of sintering aid, the domains grow gradually. In particular, it can be seen that a very large average grain size of 328 nm is obtained for a sintered body containing 0.5 wt% LiF

(Fig. 1(d)). The final grain size at ultra-low sintering temperatures of 1100 °C and 1250 °C are shown in Fig. 1(e). In both temperature conditions, the sintering aid reduces in consolidation temperature and accelerates the grain growth. The generated oxygen vacancies resulting from excessive Li^+ incorporation effectually improve the diffusivity [18]. Improvement in lattice and grain boundary diffusivity during the sintering stimulates grain coarsening and diffusional creep [19]. Fig. 1(f) shows the fractional density of the consolidated Y_2O_3 -MgO nanocomposite with a variety of sintering temperatures and amounts of LiF. At a sintering temperature higher than 1200 °C, the relative density is nearly the same regardless of the amount of LiF, but at a very low temperature of 1100 °C, there is a clear difference in the fractional density. When LiF is absent, the bulk ceramics have a low density of 91.9% because of insufficient thermal energy as a driving force to stimulate grain boundary diffusion for densification. But, when LiF is present, it shows a high density no matter how much additives are included. LiF serves as a lubricant in which Li^+ ions ameliorate the surface

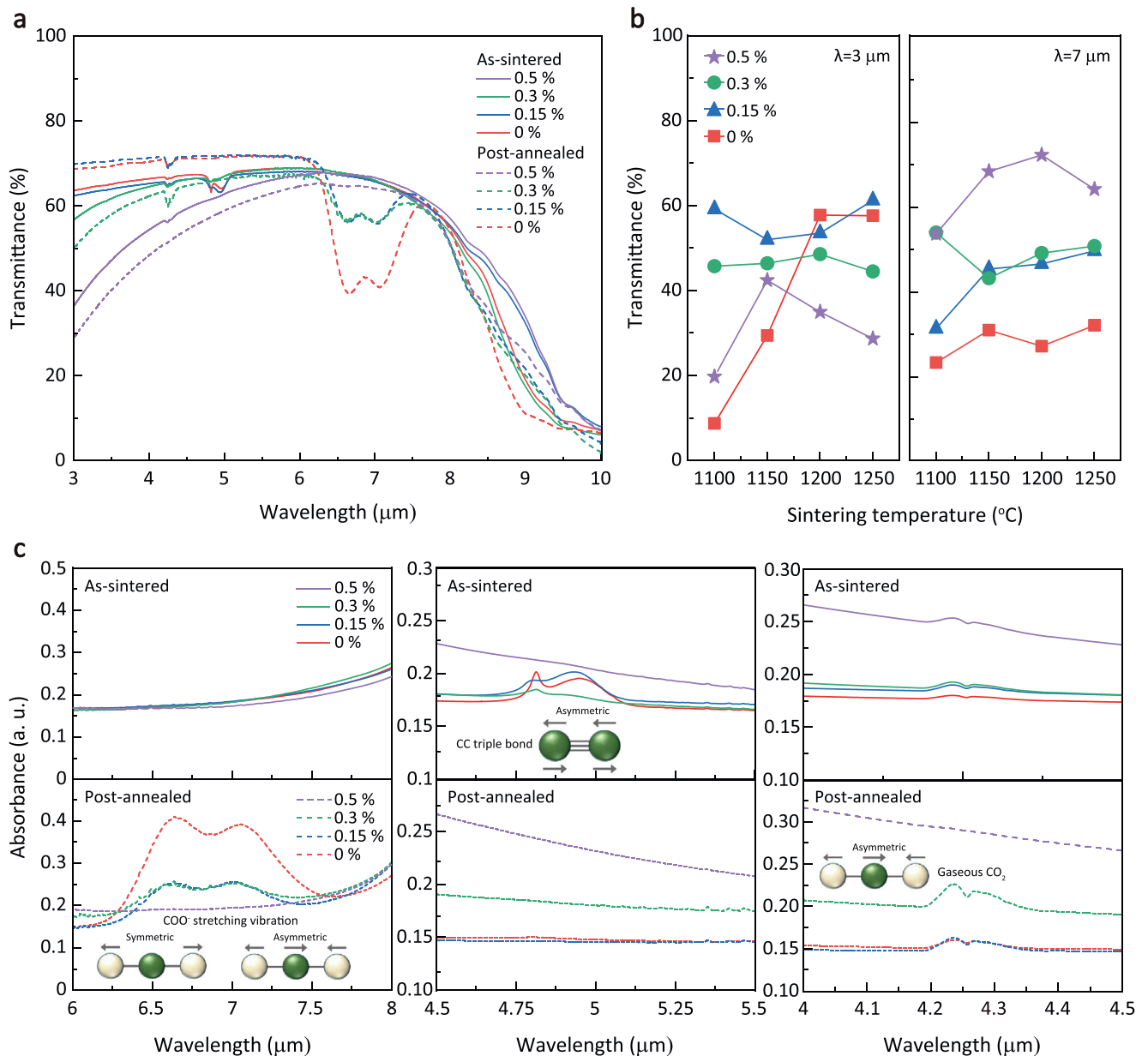


Fig. 2. (a) Infrared transmittance of $\text{Y}_2\text{O}_3\text{-MgO}$ nanocomposite sintered at 1250 $^\circ\text{C}$ with different amounts of LiF from 0 to 0.5 wt%. (b) The mid-infrared transmittance of the post-annealed samples at 3 and 7 μm wavelength regions. (c) Absorbance spectrum of the sintered $\text{Y}_2\text{O}_3\text{-MgO}$ with different amount of LiF at different wavelength regions.

activity and accelerate the surface diffusivity at the particle surface [20]. It allows the nanocomposite to have a faster shrinkage rate and high relative density at a lower temperature. Especially under the hot-pressing conditions of high pressure, LiF is evenly distributed to grain boundaries and internal pores, and the influence of highly volatile LiF on the specimen is minimized.

The mid-infrared transmittance values of the $\text{Y}_2\text{O}_3\text{-MgO}$ nanocomposite with respect to different amount of LiF sintering additive are represented in Fig. 2(a). The thickness of the polished samples was fixed at 1 mm. At a 6 μm wavelength, it can be seen that all specimens have similar transmittance regardless of whether or not LiF is added. The cut-off wavelength in the long wavelength region of the $\text{Y}_2\text{O}_3\text{-MgO}$ nanocomposite is 9 μm , which is longer than other AlON or MgAl_2O_4 transparent ceramics. At a long wavelength of 8 μm or more, the as-sintered specimens have higher transmittances than post-annealed specimens, and

there is no large difference over 9 μm . On the other hand, the transmittance in the short wavelength region where the grain size of the nanocomposite varies greatly depending on the amount of LiF added. When a small amount of LiF, 0.15 wt%, is added, the transmittance is the same as that in the case where LiF was not included. As the amount of LiF added increases gradually, the transmittance in the short wavelength region drops rapidly because LiF induces domain coarsening whereby significant grain boundary scattering degrades the optical properties in the short wavelength region. To observe how the addition of LiF affects the short and long wavelength regions, we tracked the transmittance of different consolidation temperatures and compared them as shown in Fig. 2(b). Firstly, in the 3 μm region, the transmittance of the nanocomposite with 0.15 wt% LiF remains high even though the sintering temperature is changed, but at a low sintering temperature of 1100 $^\circ\text{C}$, significant differences can be observed

depending on the presence of LiF. When there is no LiF, since the nanocomposite requires a high sintering temperature for densification, the transmittance at $3\ \mu\text{m}$ is improved with an increasing sintering temperature. However, when much LiF (0.5 wt%) is exploited at an elevated sintering temperature, excessive grain growth occurs, so that the transmittance at $3\ \mu\text{m}$ deteriorates rapidly. The most problematic phenomena in the mid-infrared transparency of the transparent ceramics fabricated through pressure-assisted sintering is that strong absorption virtually occurs in the $7\ \mu\text{m}$ region. This absorption could be generated during post-heating to eliminate residual carbon source and lattice stress, resulting in a decrease in optical properties. This detrimental absorption peak is ascribed to the stretching vibration of a carboxylate group [10,11,21]. In fact, the transmittance in the $7\ \mu\text{m}$ region depends on the amount of LiF added, as shown in Fig. 2(b). When much LiF of 0.5 wt% is added, there is little degradation of transmittance. A typical $\text{Y}_2\text{O}_3\text{-MgO}$ nanocomposite without sintering aid has a lower optical transmittance by 20% due to strong absorption resulting from carboxylate group.

To determine the influence of LiF sintering additive on various factors that cause strong absorption in the mid-infrared region, we further evaluated the absorbance according to wavelength. As shown in Fig. 2(c), the results were evaluated by dividing them into as-sintered and post-annealed $\text{Y}_2\text{O}_3\text{-MgO}$ ceramics. Firstly, the absorption peaks of the strongest 1416 and $1501\ \text{cm}^{-1}$ were largely related to the symmetric and asymmetric stretching vibration of the carboxylate group as explained above. The carboxylate group was formed when the carbon phase remaining in the initial powder is thermally decomposed during the sintering process or when glassy carbon or residual carbon components that penetrated from the graphite sleeve remained during post-annealing within the nanocomposite [22]. It is noteworthy that as more of the LiF is added, the absorption peaks in the carboxylate group decrease further. When 0.5 wt% LiF is added, in particular, the absorption peaks disappear completely, which demonstrates the same absorbance regardless of whether or not it is post-annealed. Based on these results, a large amount of LiF can effectively restrain penetration of carbon and formation of the carboxylate group.

As-sintered samples, except for those involving LiF of 0.5 wt%, show multiple absorption peaks around $2100\ \text{cm}^{-1}$. These absorption peaks are inherently relevant to stretching of the $\text{C}\equiv\text{C}$ triple bond and gaseous CO and they disappear completely after the post-annealing step [23]. In contrast, the absorption peaks around $2350\ \text{cm}^{-1}$, which are dependent on the vibration modes ($\nu_{3\text{asym}}$) of gaseous CO_2 , increase after post-annealing, except for the sample containing 0.5 wt% LiF [24]. During post-annealing in air, contaminated carbon phases and CO react with oxygen, and then transform into gaseous CO_2 . This is why the post-annealing process degrades mid-infrared transparency at 4.25 and $7\ \mu\text{m}$ [4]. Note that presence of 0.5 wt% LiF leads to less absorption by the gaseous CO during sintering, and it makes it difficult to change to entrapped CO_2 gas during the post-heating procedure because no carbon contamination takes place beforehand.

To clarify the absorption factors, the functional groups present in the $\text{Y}_2\text{O}_3\text{-MgO}$ nanocomposite were probed by X-ray photoelectron spectroscopy (XPS) after the sintering and post-annealing processes (Fig. 3). As seen in Fig. 3(a), apart from the LiF additive and post-heat treatment, all the XPS element scans of the $\text{Y}_2\text{O}_3\text{-MgO}$ nanocomposite are the same. The results of O 1s scan spectra of the samples are also the same in that the peaks are consistent with the presence of lattice and non-lattice oxygen [25]. In the C 1s spectra of the as-sintered specimen, the XPS spectrum given in Fig. 3(c), (e) and (g) shows there are four peaks related to binding energy in O-C=O , C-C=O , C-C and carbide phases, respectively [26]. In the case of the specimens before post-annealing, there were no differences in the peaks according to the binding en-

ergy in C 1s, but significant changes were confirmed after annealing. The C-C=O peak increased regardless of whether or not LiF is present. However, as shown in Fig. 3(d), when the LiF is absent, the carboxylate group (COO^-) peak is clearly seen, which indicates the strong effect of residual carbon contaminated phases. With an increasing amount of added LiF, there is mitigation of the absorption peak of the carboxylate group. Interestingly, when it added up to 0.5 wt%, this peak disappeared completely. In this case, there was no absorption peak of the carboxylate group either before or after the annealing step, which demonstrates that LiF inhibits the formation of the carboxylate group by preventing the penetration of carbon during hot-pressing. This also agrees with the FT-IR results.

Fig. 4 delineates a simple scheme of the process for the carbon cleansing effect of the LiF sintering additive for the $\text{Y}_2\text{O}_3\text{-MgO}$ nanocomposite. Carbon can easily enter the $\text{Y}_2\text{O}_3\text{-MgO}$ nanocomposite without LiF from the outside during the pressure-assisted sintering process. In addition, CO gas can be trapped in the pores inside the grain junctions, and this causes weak absorption in the $4.9\ \mu\text{m}$ mid-infrared wavelength region. After annealing, entrapped CO_2 gas which is transformed by CO gas and the carboxylate group resulting from the chemical reaction between CO_2 and metal oxide restrains transmission of incident light at $7\ \mu\text{m}$ wavelength [4]. On the other hand, it is well-known that the LiF sintering additive serves as a scavenger to eliminate impurities during the densification for MgAl_2O_4 ceramics [18]. When LiF reacts with an abundant carbon source from a graphite die and spacers, volatile CF_n phases are formed. The blocking mechanism of LiF occurs through the following reaction equation [27]:



Furthermore, liquid and gaseous LiF can physically prevent contamination from carbon atoms [14,28]. LiF gas diffuses along the grain boundary of nanocomposite ceramics and thus it protects against the penetration of carbon. Since it is difficult for the penetration of carbon impurities to occur during hot-pressing, the formation of a carboxylate group is hampered during the post-annealing process. When there are carbon contamination phases in dense ceramics, it is difficult to eliminate them by a post-annealing procedure except on the surface of samples [24]. Because these phases have a significant effect on optical properties, it is indispensable to prohibit carbon contamination during the sintering process, which makes sense in that an LiF sintering aid acts as effective carbon cleaner for the transparent nanocomposite ceramics.

We measured the Vickers hardness of the $\text{Y}_2\text{O}_3\text{-MgO}$ nanocomposites fabricated with different amounts of LiF additive. The sintering temperature was the same at $1250\ ^\circ\text{C}$. As shown in Fig. S3, the Vickers hardness of the nanocomposite relies strongly on the average grain size. A large amount of LiF leads to a larger domain size and the hardness is degraded gradually. An excessive amount of 0.5 wt% LiF results in the lowest value of 9.39. With small amount of LiF, nanograins with a large number of grain boundaries act as a physical obstacle to dislocation movement [29]. Thus, an enhanced hardness of 10.3 GPa can be obtained. It is noticeable that a small amount of LiF is effective in improving the mid-infrared transmittance without the mechanical properties deteriorating. Thus, a low amount of LiF is very advantageous in reducing unnecessary absorption by carbon impurities in the mid-infrared region and utilizing it in a wide wavelength range for polycrystalline transparent ceramics.

To put these results in perspective, the mid-infrared transparency of the $\text{Y}_2\text{O}_3\text{-MgO}$ nanocomposite ceramics fabricated with a small amount of LiF additive was significantly improved. Detailed investigation on the influence of LiF on absorption of the carboxylate group and carbon contamination in the nanocomposite during hot-pressing and post-annealing. LiF can serve as a carbon scav-

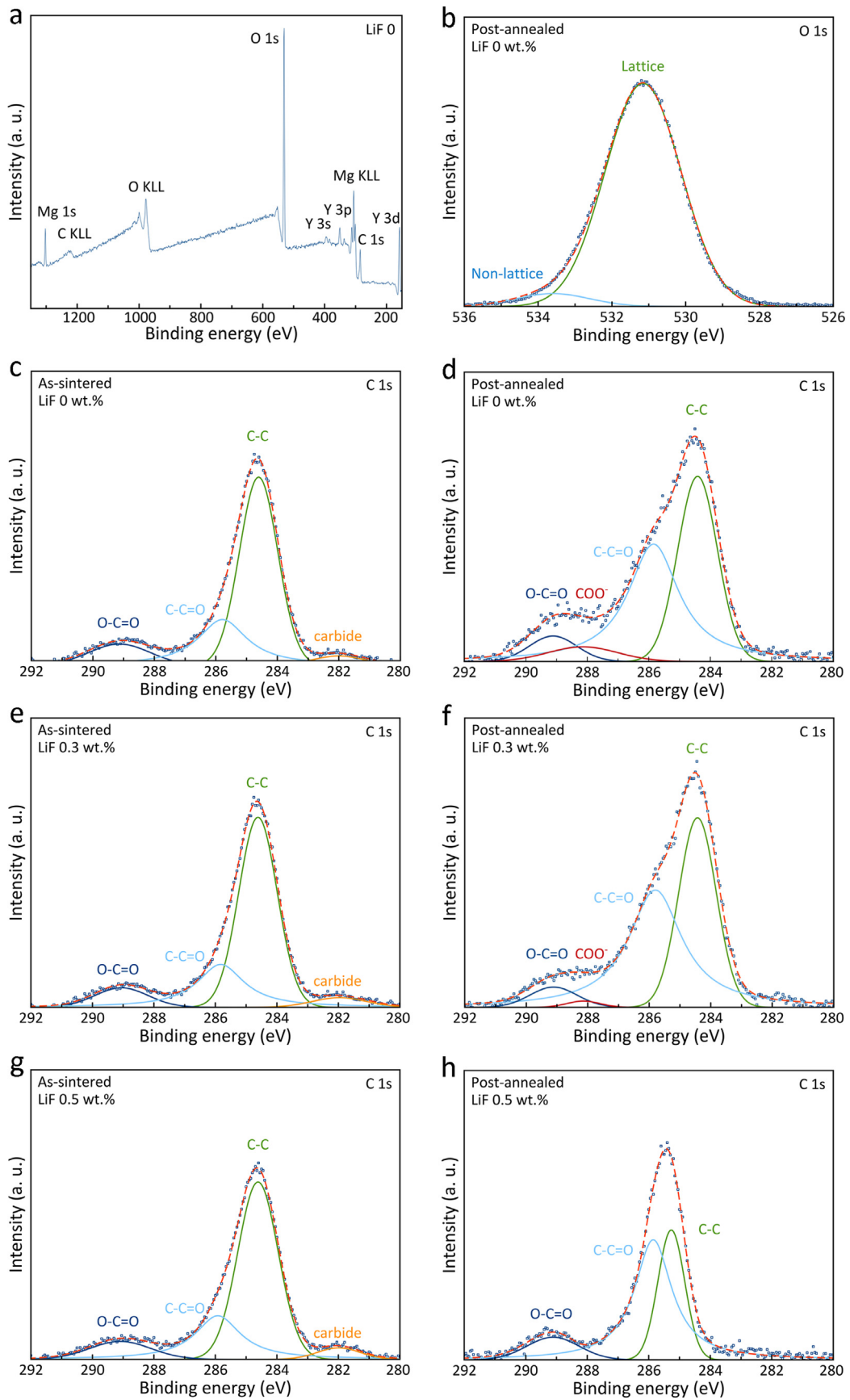


Fig. 3. X-ray photoelectron spectra of the Y_2O_3 -MgO nanocomposite ceramics. (a) Entire element scan; (b) O 1s scan spectra of the post-annealed nanocomposite without LiF additive. C 1s scan spectra of a nanocomposite without LiF (c) as-sintered and (d) post-annealed conditions; with 0.3 wt% LiF additive (e) as-sintered and (f) post-annealed conditions; with 0.5 wt% LiF (g) as-sintered and (h) post-annealed conditions.

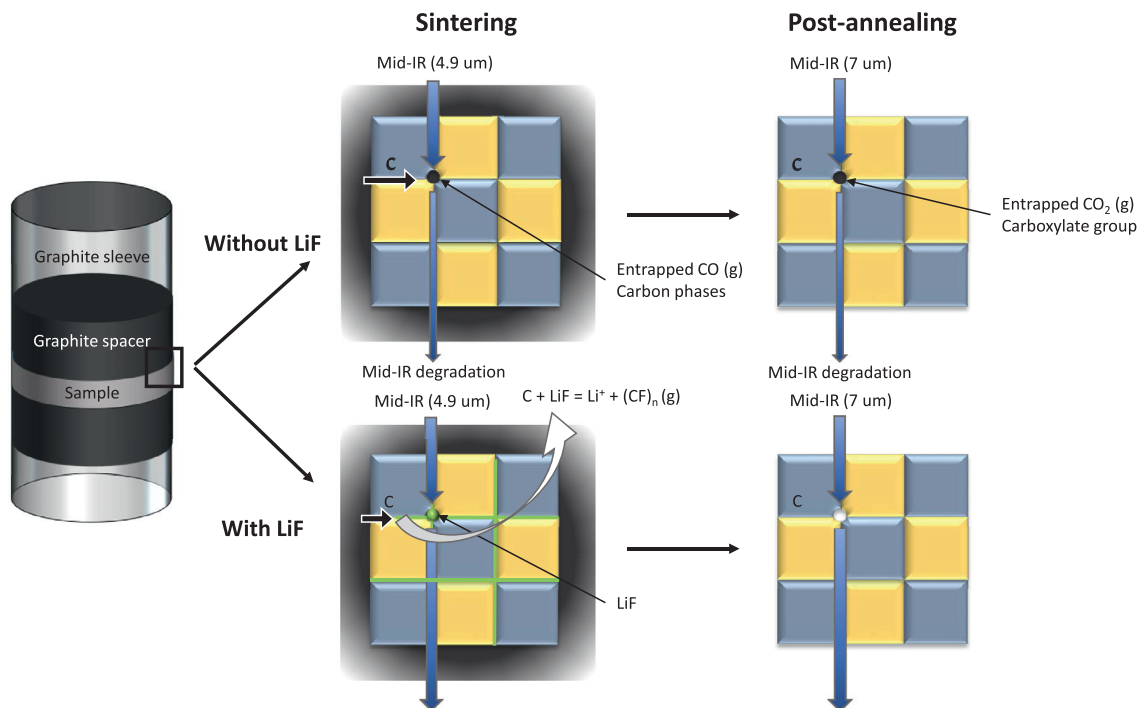


Fig. 4. Scheme of the cleansing effect of LiF for the Y_2O_3 -MgO nanocomposite transparent ceramics during the sintering and post-annealing procedure.

enger that impairs carbon contamination and formation of gaseous CO. Finally, during the post-annealing process, we observed controlled carboxylate group formation and gaseous CO_2 .

Declaration of Competing Interest

The authors declare that they have no known competing financial interests or personal relationships that could have appeared to influence the work reported in this paper.

Acknowledgments

This work was supported by the Ministry of Trade, Industry & Energy (MOTIE) of Korea (PN: 10047010) and the Agency for Defense Development (PN: UD160073BD).

Supplementary materials

Supplementary material associated with this article can be found, in the online version, at doi:10.1016/j.scriptamat.2020.05.001.

References

- [1] H.J. Ma, W.K. Jung, C. Baek, D.K. Kim, J. Eur. Ceram. Soc. 37 (2017) 4902–4911.
- [2] H.J. Ma, W.K. Jung, Y. Park, D.K. Kim, J. Mater. Chem. C 6 (2018) 11096–11103.
- [3] D.C. Harris, L.R. Cambrea, L.F. Johnson, R.T. Seaver, M. Baronowski, R. Gentilman, C. Scott Nordahl, T. Gattuso, S. Silberstein, P. Rogan, T. Hartnett, B. Zelinski, W. Sunne, E. Fest, W. Howard Poisl, C.B. Willingham, G. Turri, C. Warren, M. Bass, D.E. Zelmon, S.M. Goodrich, J. Am. Ceram. Soc. 96 (2013) 3828–3835.
- [4] S.M. Yong, D.H. Choi, K. Lee, S.Y. Ko, D.I. Cheong, Y.J. Park, S. Il Go, J. Eur. Ceram. Soc. 40 (2020) 847–851.
- [5] J. Wang, D. Chen, E.H. Jordan, M. Gell, J. Am. Ceram. Soc. 93 (2010) 3535–3538.
- [6] D. Jiang, A.K. Mukherjee, Scr. Mater. 64 (2011) 1095–1097.
- [7] M. ahsanzadeh-Vadeqani, R.S. Razavi, M. Barekat, G.H. Borhani, A.K. Mishra, J. Eur. Ceram. Soc. 37 (2017) 2169–2177.
- [8] H.J. Ma, W.K. Jung, S.-M. Yong, D.H. Choi, D.K. Kim, J. Eur. Ceram. Soc. 39 (2019) 4957–4964.
- [9] S. Xu, J. Li, H. Kou, Y. Shi, Y. Pan, J. Guo, Ceram. Int. 41 (2015) 3312–3317.
- [10] S.M. Yong, D.H. Choi, K. Lee, S.Y. Ko, D.I. Cheong, Arch. Metall. Mater. 63 (2018) 1481–1484.
- [11] J. Xie, X. Mao, X. Li, B. Jiang, L. Zhang, Ceram. Int. 43 (2017) 40–44.
- [12] G.L. Messing, A.J. Stevenson, Science 322 (2008) 383–385.
- [13] C. Wang, Z. Zhao, Scr. Mater. 61 (2009) 193–196.
- [14] A. Goldstein, J. Raethel, M. Katz, M. Berlin, E. Galun, J. Eur. Ceram. Soc. 36 (2016) 1731–1742.
- [15] K. Waetzig, T. Hutzler, J. Eur. Ceram. Soc. 37 (2017) 2259–2263.
- [16] I. Reimanis, H.J. Kleebe, J. Am. Ceram. Soc. 92 (2009) 1472–1480.
- [17] L.A. Chick, L.R. Pederson, G.D. Maupin, J.L. Bates, L.E. Thomas, G.J. Exarhos, Mater. Lett. 10 (1990) 6–12.
- [18] A. Mukhopadhyay, B. Basu, Int. Mater. Rev. 52 (2007) 257–288.
- [19] J.D. Hodge, R.S. Gordon, Ceram. Int. 4 (1978) 17–20.
- [20] R. Marder, R. Chaim, G. Chevallier, C. Estournès, J. Eur. Ceram. Soc. 31 (2011) 1057–1066.
- [21] N.A. Safronova, O.S. Kryzhanovska, M.V. Dobrotvorska, A.E. Balabanov, V.V. Tolmachev, R.P. Yavetskiy, S.V. Parkhomenko, R.Y. Brodskii, V.N. Baumer, D.Y. Kosyanov, O.O. Shichalin, E.K. Papynov, J. Li, Ceram. Int. 46 (2020) 6537–6543.
- [22] E. Irom, M. Zakeri, A.S.A.H. Zadeh, S. Safian, A. Rahbari, Micro Nano Lett. 11 (2016) 688–691.
- [23] S.T. Daniells, A.R. Overweg, M. Makkee, J.A. Moulijn, J. Catal. 230 (2005) 52–65.
- [24] K. Morita, B.N. Kim, H. Yoshida, K. Hiraga, Y. Sakka, J. Eur. Ceram. Soc. 38 (2018) 2588–2595.
- [25] C. Yang, F. Bebensee, J. Chen, X. Yu, A. Nefedov, C. Wöll, ChemPhysChem 18 (2017) 1874–1880.
- [26] S. Pletincx, K. Marcoen, L. Trotochaud, L.L. Fockaert, J.M.C. Mol, A.R. Head, O. Karslioglu, H. Bluhm, H. Terry, T. Hauffman, Sci. Rep. 7 (2017) 1–11.
- [27] S. Meir, S. Kalabukhov, N. Froumin, M.P. Dariel, N. Frage, J. Am. Ceram. Soc. 92 (2009) 358–364.
- [28] L. Esposito, A. Piancastelli, P. Miceli, S. Martelli, J. Eur. Ceram. Soc. 35 (2015) 651–661.
- [29] M. Sokol, B. Ratzker, S. Kalabukhov, M.P. Dariel, E. Galun, N. Frage, Adv. Mater. 30 (2018) 1706283.